

Educational demonstration of a spherically propagating acoustic shock

Michael B. Muhlestein^{a)} and Kent L. Gee

Department of Physics and Astronomy, N-283 Eyring Science Center, Brigham Young University, Provo, Utah 84602

Jeffrey H. Macedone

Department of Chemistry and Biochemistry, C100 Benson Building, Brigham Young University, Provo, Utah 84602

(Received 17 September 2010; revised 22 March 2011; accepted 28 March 2011)

Exploding gas-filled balloons are common chemistry demonstrations. They also provide an entertaining and educational means to experimentally verify nonlinear acoustical theory as described by the Earnshaw solution to the lossless Burgers equation and weak-shock theory. This article describes the theory, the demonstration, and the results of a propagation experiment carried out to provide typical results. Data analysis shows that an acetylene–oxygen balloon produces an acoustic shock whose evolution agrees well with weak-shock theory. On the other hand, the pressure wave generated by a hydrogen–oxygen balloon also propagates nonlinearly, but does not approach N-wave-like, weak-shock formation over the propagation distance. Overall, the experiment shows that popular demonstrations of chemical reactions can be extended from chemistry classrooms to a pedagogical tool for the student of advanced physical acoustics. © 2012 Acoustical Society of America. [DOI: 10.1121/1.3676730]

PACS number(s): 43.25.Cb, 43.28.Mw, 43.25.Vt [VWS]

Pages: 2422–2430

I. INTRODUCTION

When used appropriately, physical demonstrations of complex phenomena can inspire active learning in the classroom and provide insight into the applications of advanced mathematics.^{1,2} Examples of such demonstrations in acoustics include using a basketball to study spherical cavity resonances,³ standing waves in a Rubens flame tube,⁴ a hydrodynamic analog of the cochlea,⁵ examination of thermoacoustic principles via a Rijke tube,⁶ a gas-filled balloon lens,⁷ and acoustic levitation.⁸ This article presents a demonstration of an exploding balloon, which can be used in the explanation of phenomena important to nonlinear acoustic propagation. To increase the pedagogical utility of the demonstration, and to show how this could possibly be developed as a laboratory exercise, the theory of weak-shock propagation is reviewed and compared to experimental data.

The principal demonstration consists of a balloon filled with a stoichiometric mixture of gaseous acetylene and oxygen, which when ignited creates an acoustic shock that propagates nonlinearly. Waveforms recorded with microphones placed at various distances can be analyzed and compared with theory. Further, the acetylene–oxygen balloon results can be compared with those from a hydrogen–oxygen balloon explosion, which exhibits different nonlinear behavior. An exploding balloon demonstration is particularly useful in that it helps explain principles in a more advanced field of physics for which classroom demonstrations are not as

abundant. In addition to giving insight, the inherently entertaining nature of the demonstration can also provide motivation for introductory students to pursue more advanced studies. The demonstration can be presented along with real-world applications of acoustic shocks, including sonic booms,⁹ military jet aircraft noise,¹⁰ explosions,¹¹ Gatling guns,¹² and lithotripsy.^{13,14}

This article first presents a theoretical analysis of the propagating sound, including a discussion of the Earnshaw solution to the lossless Burgers equation and weak-shock theory.¹⁵ The development of the theoretical model is followed by a detailed description of the demonstration. Propagation data obtained for both the acetylene–oxygen and hydrogen–oxygen balloons are then analyzed and compared.

II. NONLINEAR THEORY

Theory is a wonderful source of homework exercises and a motivation for laboratory work. Throughout this section, fundamental principles of physical acoustics as they relate to the balloon demonstration are reviewed. Elements of the theoretical development could be given to an advanced acoustics class as a homework problem.

In order to model the propagation of the transient acoustic pulse generated by a compact explosive source, two models are necessary: A set of equations that appropriately describes the evolution of the pressure waves and a model for the source waveform. The use of the source waveform in the propagation model, which relies on the Earnshaw solution to the lossless Burgers equation and weak-shock theory, results in theoretical expressions that can be used to compare with experimental data obtained from the physical demonstration.

^{a)}Author to whom correspondence should be addressed. Electronic mail: mimuhle@gmail.com

A. Propagation model

1. The Earnshaw solution to the Burgers equation

This section describes the theory^{15,16} that is used to model the continuous portion of the propagating transient. As this theory is not new and our development is similar to that of Blackstock *et al.*,¹⁶ it is largely included for completeness in this education-oriented article. In addition, although our demonstration involves the propagation of finite-amplitude spherical waves, it is easier to develop the plane-wave solution and then convert it into spherical coordinates afterward, as done by Blackstock.¹⁷

The model equation used to describe the nonlinear evolution of the acoustic pressure p (hereafter just called the pressure) is the lossless, planar Burgers equation,

$$\frac{\partial p}{\partial x} = \frac{\beta}{\rho_0 c_0^3} p \frac{\partial p}{\partial \tau}, \quad (1)$$

where x is the distance from the source, β is the parameter of nonlinearity (1.201 for air), ρ_0 is the ambient air density, c_0 is the small-signal sound speed, and τ is the retarded time, $t - x/c_0$. This equation is valid for continuous waveforms, which means that once shocks form, it no longer describes propagation of the entire wave.

An often used solution to the lossless Burgers equation is the Earnshaw solution,¹⁶ which may be written as

$$p = f(\phi), \quad (2)$$

$$\phi = \tau + \frac{\beta x p}{\rho_0 c_0^3} = \tau + \frac{\beta x}{\rho_0 c_0^3} f(\phi). \quad (3)$$

The variable ϕ is the nonlinearly distorted time scale and is called the Earnshaw phase variable by Blackstock *et al.*¹⁶ In addition to facilitating analytical solutions, ϕ is convenient for numerical solutions of the Burgers equation,^{10,18,19} as the initial waveform values do not change, only the time at which they occur. Physically, the pressure-dependent distortion of the Earnshaw solution in Eq. (3) describes how the compressions travel faster than rarefactions in the waveform steepening process prior to shock formation.

The Earnshaw solution can be used as a pedagogical tool or as part of a homework exercise where students can use the solution to distort a discretely sampled waveform. For example, the Earnshaw solution can be compared with the Fubini series solution²⁰ for a monofrequency source described by $f(\phi) = p_0 \sin(\omega\tau)$ at $x = 0$, where ω is the angular frequency. By Eq. (3), $\phi = \omega\tau + \beta p_0 \omega x \sin(\phi) / \rho_0 c_0^3$. Plotting the solution to the pressure as a function of the nondimensional distance, $\sigma = \beta p_0 \omega x / \rho_0 c_0^3$, is instructive. Normalized pressure waveforms for six values of σ are displayed in Fig. 1.

Notice in Fig. 1 that a portion of the waveform slope first becomes perfectly vertical at $\sigma = 1$, causing $\sigma = 1$ to be referred to as the shock formation distance and σ as the distance relative to the shock formation distance. Having students plot the solution for $\sigma > 1$ can be used to motivate a discussion of weak-shock theory¹⁶ and the equal-area rule,

described in further detail in the following. Figure 1 shows the shock propagation relative to the Earnshaw solution for three values of $\sigma > 1$.

2. Weak-shock theory

For $\sigma > 1$, the continuous Earnshaw solution cannot be used in the multivalued regions. Weak-shock theory is instead required. Weak-shock theory is based on three assumptions. First, shocks are “weak,” which is described further in the following. Second, losses are only considered at the shocks (i.e., the propagation of the continuous portion of the waveform may be considered lossless). Third, shocks are ideal discontinuities. Using these assumptions with the Rankine-Hugoniot shock relations,²¹ one finds that shocks propagate at a velocity of

$$v_{\text{sh}} = \frac{\beta}{\rho_0 c_0} \frac{(p_1 + p_2)}{2}, \quad (4)$$

where v_{sh} is the velocity of the shock, and p_1 and p_2 are the pressure ahead of the shock and behind the shock, respectively. Note that this means that shocks propagate at speeds different from the continuous portions of the waveform surrounding the shock. In order to find the location of a shock, the relation for the retarded “slowness” of the shock [see Eq. (163) in Ref. 16],

$$\frac{d\tau_{\text{sh}}}{dx} = -\frac{\beta}{\rho_0 c_0^3} \frac{(p_1 + p_2)}{2}, \quad (5)$$

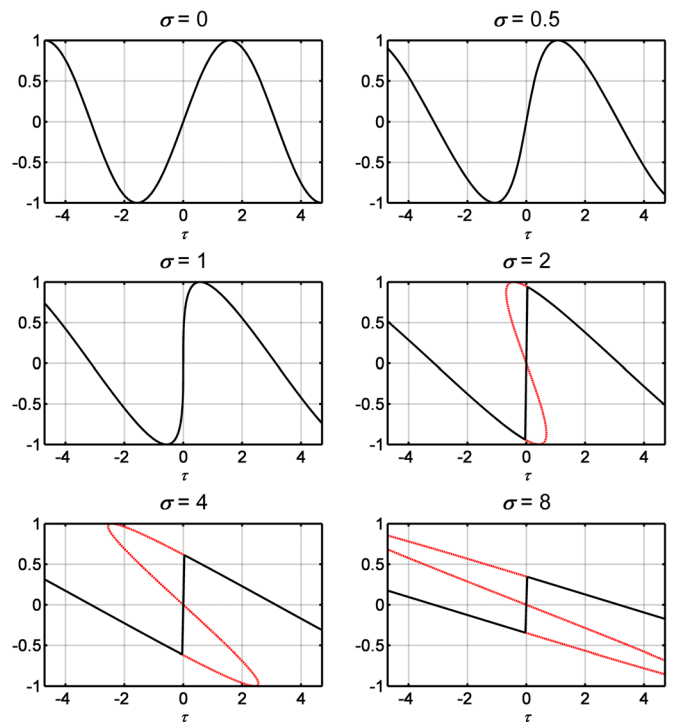


FIG. 1. (Color online) Nonlinear propagation of an initially sinusoidal wave of frequency ω according to the Earnshaw solution to the planar, lossless Burgers equation. The variable σ is a dimensionless distance where $\sigma < 1$ represents the preshock region. The multivaluedness of the Earnshaw-derived pressure for $\sigma > 1$ can be used to motivate a discussion of weak-shock theory. The amplitude has been normalized (p/p_0).

where τ_{sh} is the retarded time of arrival of the shock, is a more useful form of Eq. (4). To use Eq. (5), p_1 and p_2 are found from Eqs. (2) and (3) to be

$$p_1 = f(\phi_1), \quad \phi_1 = \tau + \frac{\beta x p_1}{\rho_0 c_0^3}, \quad (6)$$

$$p_2 = f(\phi_2), \quad \phi_2 = \tau + \frac{\beta x p_2}{\rho_0 c_0^3}. \quad (7)$$

Equations (2), (3), and (5)–(7) are an adequate set of equations to model the finite-amplitude pressure wave propagation. Note that implicit in the use of Eqs. (6) and (7) is the equal area rule, which states that the shock separates equal areas as defined by the Earnshaw solution. (A demonstration of the equal area rule can be seen in Fig. 1.)

As with any model, it is important to understand the limitations of weak-shock theory. One of the three assumptions discussed previously is that shocks are “weak.” Temkin²² studied errors associated with the weak-shock approximation in the expression for the entropy change across shocks in planar sawtooth waves at sea level. Used as the figure of merit was the shock strength, defined as

$$\delta = \frac{p_2 - p_1}{p_1 + p_{\text{amb}}}, \quad (8)$$

where p_{amb} is the ambient pressure. The upper bound of acceptable errors was found to be $\delta = 0.1$, which corresponds to a root mean square sound pressure level of 165 dB re 20 μPa . Note that Blackstock²³ used a different criterion in his examination of weak-shock theory limits. He employed the peak acoustic Mach number, $\text{Ma} = u_0/c_0$, where u_0 is the peak particle velocity, with weak being defined as $\text{Ma} < 0.1$. This yields an upper bound for planar sawtooth waves of 174 dB re 20 μPa ($\delta = 0.329$).²⁴

Regardless of the criterion used to obtain the weak-shock theory upper bound, neither result applies strictly to the waveform of an exploding gas-filled balloon. One cause is geometric spreading, which serves to rapidly reduce the peak pressure for the same propagation range. This would effectively increase the upper bound of weak-shock theory. Another cause is the nature of the waveform itself, which is an asymmetric transient rather than a symmetric, stationary signal. To the authors’ knowledge, the theoretical upper limits of weak-shock theory for a spherically propagating transient impulse have not been determined as has been done for the planar sawtooth wave. Therefore, the appropriateness of the weak-shock theory model for this case is established empirically by the level of agreement between predictions and experiment.

B. Explosion model

A commonly used model for an acoustic impulse created by an explosion is the modified Friedlander equation,¹¹ written as

$$p(t) = p_0(1 - t/T^+)e^{-bt/T^+}, \quad (9)$$

where p_0 is the peak shock pressure value, T^+ is duration for which the pressure value is positive, and b is a fitting

parameter. However, this equation is not as well suited for analytical analysis as a shock followed by an exponentially decaying tail, which is sufficient to illustrate features of interest. Thus, the source model employed in this study is

$$f(t) = \begin{cases} p_0 e^{-t/t_0}, & t > 0 \\ 0, & t < 0 \end{cases}, \quad (10)$$

where t_0 is the initial e^{-1} decay time of the tail.

The solution of Eqs. (2), (3), and (5)–(7) with Eq. (10) as the source was first found with a finite-difference formulation by Rogers.²⁵ Blackstock²⁶ approached the problem with an analytical formulation and found expressions for many key elements, although he did not provide a solution for the entire pressure waveform. The present formulation is included for educational value, as it solves for the full waveform using both the Earnshaw solution and weak-shock theory.

There are two semi-infinite portions of the wave that are continuous: Before the shock and after the shock. Because $p = 0$ before the shock, the Earnshaw phase variable is simply $\phi = \tau$. For the portion behind the shock, the Earnshaw solution yields

$$p = p_0 e^{-(\tau + Cx)/t_0}, \quad (11)$$

where the substitution of $C = \beta/\rho_0 c_0^3$ is made. Equation (11) can be rewritten as

$$ze^z = \frac{p_0}{t_0} Cx e^{-\tau/t_0}, \quad (12)$$

where $z = Cx p/t_0$. The solution to Eq. (12) is

$$z = W\left(\frac{p_0}{t_0} Cx e^{-\tau/t_0}\right), \quad (13)$$

where W is the Lambert W function.²⁷ Thus, the waveform after and before the shock may be written as

$$p(x, \tau) = \begin{cases} t_0 W\left(\frac{p_0}{t_0} Cx e^{-\tau/t_0}\right) / Cx, & \tau > \tau_{\text{sh}} \\ 0, & \tau < \tau_{\text{sh}} \end{cases}. \quad (14)$$

As mentioned earlier, Eq. (14), which is derived from the Earnshaw solution, is only valid for continuous portions of the waveform, and weak-shock theory is necessary to find τ_{sh} in terms of x . This requires that Eqs. (5)–(7) be solved. The source waveform in Eq. (10) allows one to immediately see that the pressure ahead of the shock is $p_1 = 0$. This means that the peak pressure of the shock, which we call p_{sh} , is identical to p_2 . Solving for p_{sh} in a functional form is more difficult (and is likely worthy of a graduate-level homework exercise²⁸) but Blackstock²⁶ found it to be

$$p_{\text{sh}} = \frac{\sqrt{1 + 2p_0 Cx/t_0} - 1}{Cx/t_0}. \quad (15)$$

With a solution for p_{sh} , Eqs. (2) and (3) can be evaluated at ϕ_{sh} to find τ_{sh} as

$$\tau_{sh} = t_0 - t_0 \sqrt{1 + 2p_0 Cx/t_0} - t_0 \ln \left(\frac{\sqrt{1 + 2p_0 Cx/t_0} - 1}{p_0 Cx/t_0} \right). \quad (16)$$

Figure 2 illustrates how the waveform decays and spreads as it propagates according to Eqs. (14) and (16). Because the Lambert W function in Eq. (14) cannot be written directly in terms of elementary functions, an approximation is necessary. Rogers²⁵ used Newton's method to find an approximation for the pressure wave in terms of elementary functions. To generate the results in Fig. 2, the MATLAB[®] lambertw.m²⁹ function was used. The 1–4 m propagation range was selected in order to be the same as the spherical case shown subsequently.

Equations (14) and (16) describe the evolution of the source waveform in Eq. (10) for planar propagation. To convert this result into spherical coordinates, Eq. (14) is multiplied by r_0/r and in Eqs. (14) and (16) the variable x is replaced with $r_0 \ln(r/r_0)$. In this replacement, r_0 is the reference radius at which p_0 and t_0 are known and r is the distance from the source origin.²⁴ In spherical coordinates, the expressions for $p(x, \tau)$ and τ_{sh} become

$$p(r, \tau) = \begin{cases} \frac{r_0 p_0 t_0 W(\eta \ln(r/r_0) e^{-\tau/t_0})}{r \eta \ln(r/r_0)}, & \tau > \tau_{sh} \\ 0, & \tau < \tau_{sh} \end{cases}, \quad (17)$$

$$\tau_{sh} = t_0 - t_0 \sqrt{1 + 2\eta \ln(r/r_0)} - t_0 \ln \left(\frac{\sqrt{1 + 2\eta \ln(r/r_0)} - 1}{\eta \ln(r/r_0)} \right), \quad (18)$$

$$\eta = \frac{p_0 \beta r_0}{t_0 \rho_0 c_0^3}, \quad (19)$$

where τ is now defined as $t - (r - r_0)/c_0$.

Also of interest is the peak pressure value in spherical coordinates, obtained by transforming Eq. (15) as described previously. The peak pressure, p_{sh} , is given by

$$p_{sh} = \frac{r_0 p_0 \sqrt{1 + 2\eta \ln(r/r_0)} - 1}{r \eta \ln(r/r_0)}. \quad (20)$$

Figure 3 illustrates how the waveform spreads as it propagates according to Eqs. (17)–(20). Note that the attenuation of the shocks in the spherical case is much greater than in the planar case (Fig. 2) and, consequently, the temporal elongation of the waveform is less.

It is important to remember that Eqs. (17)–(20) only describe the evolution of the shock with decaying exponential tail under conditions that satisfy weak-shock theory. In addition to the weak requirement described earlier, there are various other factors that can lead to discrepancy between experiment and theory for a real fluid. Molecular relaxation and thermoviscous absorption will cause the shock rise time to be finite.³⁰ Further, as distance increases, the absorptive processes will result in ordinary losses affecting the entire waveform.³¹ Finally, dispersion would also be an important consideration over large distances.³²

III. DEMONSTRATION AND EXPERIMENT

This section discusses the basic chemistry associated with the exploding balloon demonstration and describes how the demonstration is carried out. Discussed also is an experiment that was performed as a comparison with the theory described in Sec. II.

A. Chemistry overview

Nonlinearly propagating pressure waves can be generated by chemical reactions in the combustion of two easily obtainable fuels: Hydrogen (H_2) or acetylene (C_2H_2). In any chemical reaction, reactant species experience a rearrangement of atoms or ions to create new product species, as bonds are broken and new ones are formed. The total energy change for the reaction is the difference between the energy required to break bonds and the amount of energy released in the formation of new bonds. In the case of the combustion reactions used here, there is a net release of energy; more energy is released in the forming of new, more stable bonds

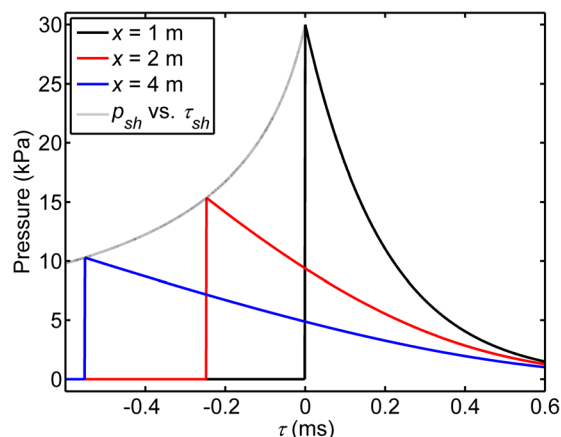


FIG. 2. (Color online) Theoretical evolution of a propagating planar shock with exponential tail. In this case, $t_0 \sim 0.2$ ms and $p_0 = 30$ kPa. The choice of p_0 is derived from the acetylene–oxygen balloon experiment.

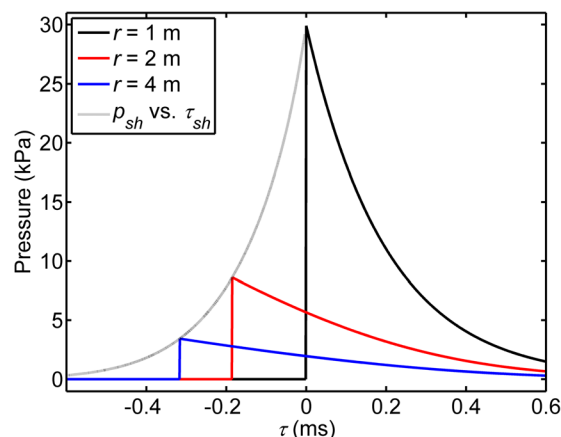
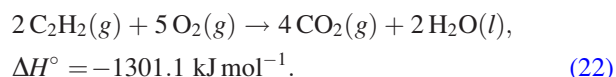
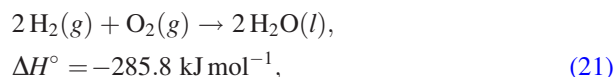


FIG. 3. (Color online) Theoretical evolution of a spherically propagating shock with exponential tail. In this case, $t_0 \sim 0.2$ ms, $p_0 = 30$ kPa, and $r_0 = 1$ m.

than was required to initially break the bonds between reactant species.

One measure of the amount of energy released in a reaction is enthalpy change (ΔH°); enthalpy is a measure of the heat energy in a reaction. The heat energy released in a reaction heats the reaction gases, which increases the velocity of the gas molecules and generates a pressure wave at the site of the explosion. The following reactions outline the combustion reactions for the fuels used:



The enthalpy values are negative to indicate that heat energy is released from the reaction.

Note that even though the same numbers of fuel moles are used in reactions (21) and (22), there is a significant difference in the enthalpy change in these two reactions. The reason for this is not that more bonds are formed than are broken. In fact, the same numbers of bonds are broken as are formed for both reactions. The disparity in energy between the two above-mentioned reactions arises from differences in the types of bonds that are formed. For example, approximately twice as much energy is released in the formation of a carbon–oxygen bond as that of a hydrogen–oxygen bond. The acoustical analysis below shows that acetylene–oxygen explosions have significantly larger pressure waves. This is due to the enthalpy considerations mentioned above and also because this large amount of heat energy is released on a faster time scale than in the hydrogen–oxygen case. A more complete discussion of the reaction kinetics of these two reactions is beyond the scope of this article.

B. Demonstration description

To prepare the balloons, reactions (21) and (22) were used to determine the appropriate amount of oxygen (O_2) for a complete burn of the fuel. For combusting hydrogen (H_2), 0.370 mol of hydrogen with 0.185 mol of oxygen was used (total balloon diameter of 31.1 cm). For acetylene combustion, 0.057 mol of acetylene with 0.143 mol of oxygen was used (total balloon diameter of 22.1 cm). The amount of fuel used in these experiments was a matter of convenience.

A predictable demonstration relies both on the proper amount of fuel and ratio of fuel to oxygen. Because accurate delivery of gases is difficult, the volume of gas required was converted to the diameter of a sphere. Plastic tubing was then shaped to form a ring of the appropriate diameter required for a certain volume as calculated by the ideal gas law. Latex balloons, manufactured to be more spherical than typical tear-drop-shaped party balloons, are then filled directly from compressed gas cylinders until the balloon walls just touch the inside diameter of the plastic ring. Two plastic tubing rings were prepared for each type of balloon; a smaller ring to ensure the proper amount of fuel and a sec-

ond, larger ring to indicate the amount of oxygen to be added to the initial amount of fuel to create the appropriate mixture. Once the gaseous mixture is prepared, precautions should be observed. These include wearing ear and eye protection and keeping the balloons well away from heat sources.

The balloons are ignited by using a wand consisting of surgical tubing attached to a 1 m hollow stainless steel rod. The surgical tubing is then connected to a natural gas supply and the wand lit in order to ignite the balloon. Whatever mechanism is used to anchor the balloon should be secured so that it will not become a projectile. When initiating the reaction, presenters should hold the flame wand with an outstretched arm to maintain a 2 m distance from the explosion. This is both to reduce the peak acoustic levels to which the presenter is exposed and to remain well outside the explosion. The maximum acetylene–oxygen fireball diameter is approximately 80 cm in diameter (see Fig. 4) and the hydrogen–oxygen fireball diameter is ~ 1 m. Due to the explosive nature of the demonstration and the potential for balloon piece projectiles, a lab coat and eye protection should be worn by the presenter.

Because there is the potential for significant auditory hazard, some additional comments regarding hearing protection are merited. Recent experiments on the levels generated by hydrogen–oxygen balloons have been discussed by Gee

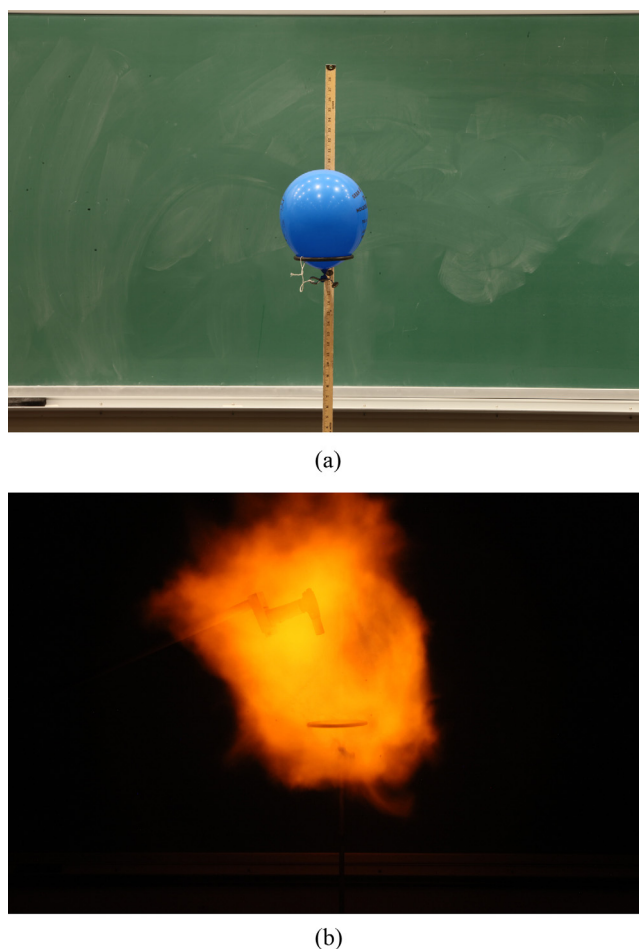


FIG. 4. (Color online) Before (a) and during (b) pictures of an acetylene–oxygen balloon explosion in a classroom. Ruler in (a) is present for scale. The maximum explosion radius is ~ 79 cm.

*et al.*³³ Properly worn double hearing protection (meaning earplugs and muffs) can provide ~ 50 dB attenuation for impulse noise³⁴ and reduce peak levels to below the critical threshold of 140 dB re 20 μ Pa for the demonstrator and viewers. Note that this demonstration can also serve as an opportunity to teach students about the importance and proper wearing of hearing protection.

If this demonstration is to be carried out in a classroom environment, thought should be given to the impact of room reflections. In order to prevent the initial acoustic impulse and reflections from overlapping in time, the distance from the explosion to any hard surfaces should be greater than ~ 30 cm. This distance is calculated from the duration of the positive pressure impulse of the explosions at the 3.46 m microphone. This will allow for clear analysis of an experiment conducted in a regular classroom (not just in an anechoic chamber, as used in the propagation experiment presented here). As a final practical note, the acetylene–oxygen balloons should be used within ~ 20 min after preparation as the acetylene diffuses through the latex balloon wall at a sufficiently fast rate that reproducibility and balloon volume are reduced.

C. Experiment setup

This section describes the acetylene–oxygen and hydrogen–oxygen balloon experiment carried out to examine their nonlinear propagation characteristics. In order to focus on spherical spreading and minimize other effects due to reflections, the experiment was conducted in the large fully anechoic chamber at Brigham Young University with working dimensions of $8.71 \times 5.66 \times 5.74$ m. It should be noted that the chamber has an upper frequency limit (~ 20 kHz) for which it is anechoic. This means that some reflections from the room at the very high frequencies associated with shocks are unavoidable, but these reflections do not impact the waveform propagation characteristics of primary importance to this article.

As shown in Fig. 5, microphones were placed at 1.02, 1.17, 1.32, 1.63, 1.93, 2.85, and 3.46 m from the center of the balloon for the acetylene and oxygen balloon test. The location of the closest microphone was chosen to avoid clipping of the data. The remaining microphones' locations were weighted toward closer to the balloon, but were somewhat arbitrarily chosen. For the hydrogen–oxygen balloon test, the balloon was 0.305 m (1.00 ft) farther from all of the microphones. Because the hydrogen–oxygen balloon was not quite so loud the greater distance allowed for the nonlinear effects to become more apparent. As the center of the balloon is not

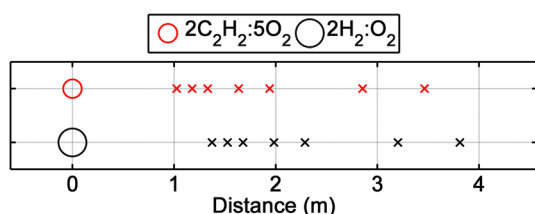


FIG. 5. (Color online) Schematic showing microphone locations relative to the acetylene–oxygen ($2C_2H_2:5O_2$) and hydrogen–oxygen ($2H_2:O_2$) balloons for the results described in this article.

necessarily the exact source location, the value of r_0 is a source of potential error in comparing the model and experiment. The microphones were suspended from a network of cotton twine strung between two stands in order to minimize the number of possible scattering sources. The microphones used were 3.18 mm (1/8 in.) G.R.A.S. 40DD microphones (G.R.A.S. Sound and Vibration, Holte, Denmark), except for the most distant microphone, which was a 6.35 mm (1/4 in.) G.R.A.S. 40BD microphone. The grid caps of the microphones were removed in order to remove any shock-induced high-frequency resonances of the cavity between the grid cap and the microphone diaphragm.³⁵ Because diffraction due to microphone orientation has a significant effect on the measurements of shock amplitude,^{35,36} the microphones were placed as near as possible to grazing incidence. Uncertainty in the orientation and any shadowing and scattering from upstream microphones are possible sources of error in the measurement of the shock amplitude.

During the experiments, time waveform data were acquired with a National Instruments (Austin, TX) PXI-based system using 24-bit PXI-4462 cards controlled by LABVIEW-based (National Instruments, Austin, TX) software. The data were acquired at a rate of 204 800 samples/s (4.9 μ s/sample). Post-processing of the data was performed using MATLAB[®].

IV. RESULTS

Shown in this section are time waveform measurements for both the acetylene–oxygen and hydrogen–oxygen balloons. Presented in Fig. 6 are the measured acetylene–oxygen balloon waveforms aligned at the zero crossing, which propagates at the ambient speed of sound and thus does not change relative to the retarded time. The measured peak pressure, p_{pk} , of the acetylene–oxygen balloon at 1.02 m was 31.03 kPa. This is equivalent to a peak sound pressure level,³⁶ $L_{pk} = 20 \log_{10}(p_{pk}/20 \mu\text{Pa})$, of 183.8 dB re 20 μ Pa.

The peak pressure for the hydrogen–oxygen balloon shown in Figs. 3 and 7. At 1.37 m, 26 kPa ($L_{pk} = 164.2$ dB re 20 μ Pa) is substantially less than that of the acetylene–oxygen balloon at 1.32 m, 16.0 kPa ($L_{pk} = 178.1$ dB re 20 μ Pa), and occurs over a greater time scale. Note that for this balloon, aligning the initial impulse also aligns the

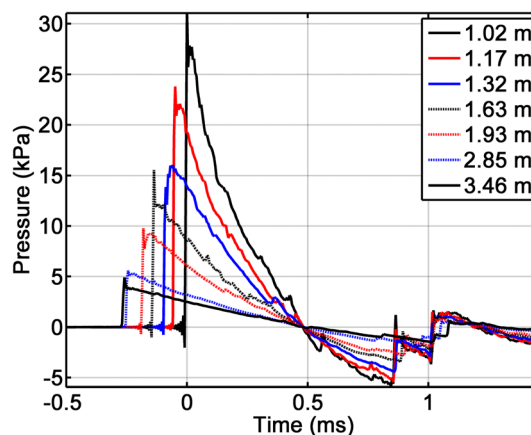


FIG. 6. (Color online) Measured time waveforms, aligned at the impulse zero crossing, for an acetylene–oxygen balloon.

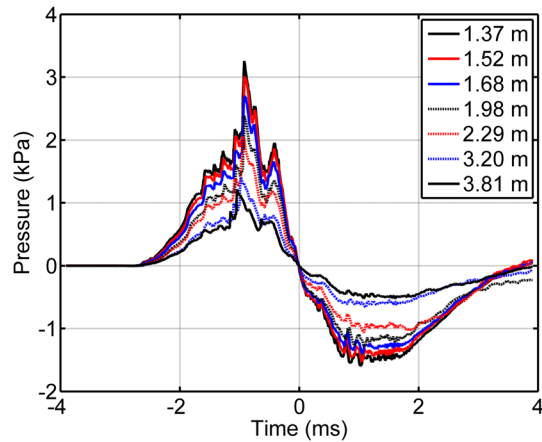


FIG. 7. (Color online) Measured time waveforms for a hydrogen–oxygen balloon.

waveform at the zero crossing, as shown in Fig. 7. Comparing Fig. 7 to Fig. 6 shows that this dual alignment, or lack of time-scale elongation, is a major difference between the two explosions, as is the lack of a single, significant shock in Fig. 7.

V. ANALYSIS AND DISCUSSION

The results of the previous section provide for discussion as to the effects of shocks and nonlinear propagation appropriate for an advanced acoustics course. First, although the upper bounds of weak-shock theory for this propagation scenario are not well established, a calculation of the qualitative “weakness” of the shock for the acetylene–oxygen balloon is worthwhile. Application of Eq. (8) for a peak pressure of 31.03 kPa and an ambient pressure of 88 kPa in Provo, UT yields $\delta = 0.341$. The peak acoustic Mach number, assuming locally planar behavior, is 0.22. These exceed the limits for the planar sawtooth wave discussed previously, but are still small. Further, as is now shown, the weak-shock model developed in Sec. II is an acceptable pedagogical tool that can be applied to the exploding acetylene–oxygen balloon demonstration.

The theory of a propagating weak shock with an exponential tail predicts that the peak amplitude, p_{sh} , rolls off according to Eq. (20) and its retarded time of arrival, τ_{sh} , evolves according to Eq. (17). Because the zero crossing travels at the ambient sound speed and its retarded time does not change, it is a useful reference point from which to examine the amplitude decay and waveform time-scale increase. However, to compare with experiment, Eqs. (18) and (20) require values for r_0 , p_0 , and t_0 . The value for r_0 used is the distance from the source origin, approximated as the center of the balloon, to the first microphone. The values of p_0 and t_0 are taken directly from the measured data. The peak pressure of the closest microphone is used as p_0 and the time it takes for the pressure to decay to $1/e$ of the peak value is used for t_0 .

In Fig. 8, the peak sound pressure level calculated from the peak pressures from Fig. 6 are displayed with the theoretical prediction for L_{pk} decay calculated from Eq. (20). Ordinary spherical spreading is also included for reference.

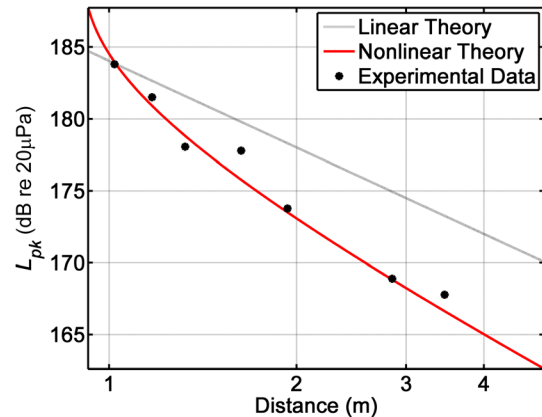


FIG. 8. (Color online) Measured peak sound pressure level (L_{pk}) from the acetylene–oxygen balloon as a function of distance with theoretical linear and nonlinear curves.

Inspection of Fig. 8 shows that the experimental data diverge quickly and substantially from the linear theory. At 3 m from the source, the excess attenuation of the peak is greater than 6 dB. This means that in order to get any sort of reasonable prediction for the peak pressure value as a function of distance, nonlinear theory must be used. Note further that the overall agreement between the experimentally measured pressures and the weak-shock theory prediction suggests that application of this model is appropriate.

Figure 9 shows the measured time waveforms from Fig. 6 with respect to retarded time with the zero crossing as a reference point. Also shown in Fig. 9 is the theoretical p_{sh} versus τ_{sh} curve predicted from Eqs. (18) and (20). The waveform elongation in the propagation data is clearly evident. The positive impulse duration at 1.02 m is slightly less than 0.5 ms, but at 3.46 m has increased to ~ 0.8 ms. Further, a reasonable match between the experiment and the model prediction is obtained. Some possible causes for the differences between measurement and theory, particularly related to the shock measurement, are now discussed.

Although the experimental waveform evolution generally agrees with p_{sh} versus τ_{sh} predicted from Eqs. (18) and (20), there are differences that were fairly consistent for the several balloon explosions measured. Examination of the time waveforms and comparison with data shown by Gabrielson *et al.*³⁵ suggests that the inexactness in the peak pressure measurement is primarily due to diffraction caused by slight pressure microphone orientation errors. Another possible source of error is the Gibbs-phenomenon artifacts present in Fig. 9. The pressure oscillations at the base of the shocks are caused by the brick-wall nature of the oversampling/decimation used in the analog-to-digital converter of the data acquisition boards. [Note that transient response can be reduced by using an analog lowpass (e.g., Bessel) filter prior to digitization, but which necessarily reduces the measurement bandwidth, thereby increasing the rise time of the shock.] These oscillations may also exist at the top of the shocks as well, which could cause some overestimation of the peak pressure values.

The pedagogical nature of Figs. 6 and 8 is enhanced when compared with results from the hydrogen–oxygen

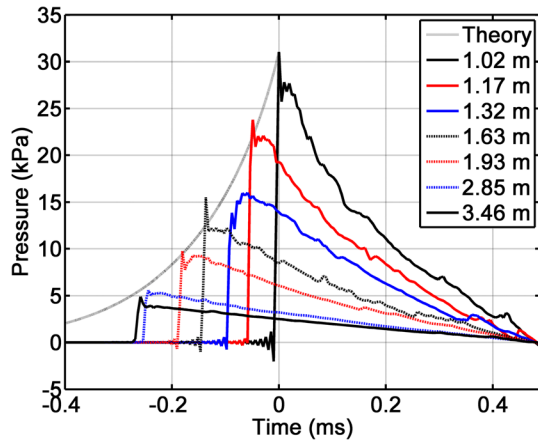


FIG. 9. (Color online) Measured waveforms of the acetylene–oxygen balloon compared with the theoretical evolution of the shock amplitude and time.

balloon. In contrast to the shock that was formed with the acetylene–oxygen balloon the hydrogen–oxygen balloon has a much more gradual transition from ambient pressure to the waveform peak. It has been already noted in the discussion of Fig. 7 that the same time-scale elongation observed in the acetylene–oxygen explosion is not observed in the hydrogen–oxygen explosion. However, one can still use these latter results to observe nonlinear behavior and distinguish it from the weak shock-like behavior of the acetylene–oxygen balloon.

To more clearly examine the nonlinear evolution of the time waveform for the hydrogen–oxygen balloon in Fig. 7, the waveforms of the closest (1.37 m) and farthest (3.81 m) microphones were multiplied by their respective distances from the assumed origin, thereby removing spherical spreading. The positive portions of the resultant waveforms are shown in Fig. 10. Notice the consistency of the location of the zero crossings before and after the initial compression wave combined with advancement of the greater amplitude portions forward in time. This clearly shows nonlinear steepening of the hydrogen–oxygen waveform, but in the preshock region, which is very different nonlinear behavior than the acetylene–oxygen balloon exhibits. Note that students could

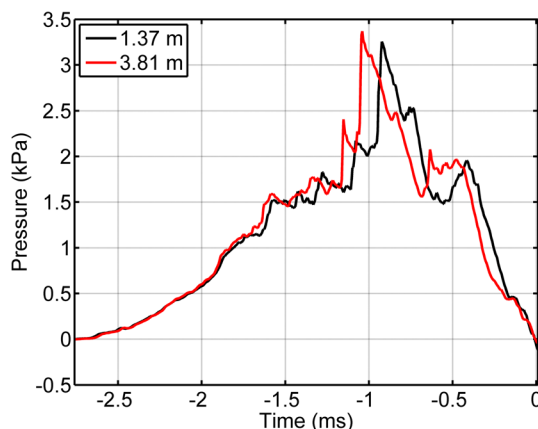


FIG. 10. (Color online) Measured waveform of a hydrogen–oxygen balloon from Fig. 7 at the closest and farthest microphones with spherical spreading removed.

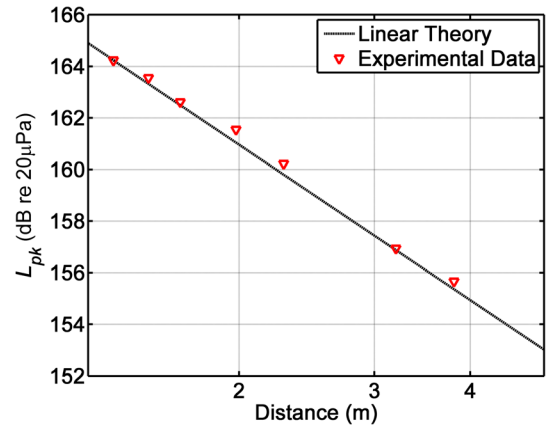


FIG. 11. (Color online) Measured peak sound pressure level (L_{pk}) of the hydrogen–oxygen balloon with linear theory, confirming data were taken in the preshock region.

compare results similar to Fig. 10 with an Earnshaw solution prediction to examine the dependence of nonlinearity on the nature of the geometric spreading. In this case, the nonlinear advancement of the peak pressure that occurs at ~ -1.0 ms is approximately half what it would be if the propagation of the wave were planar rather than spherical.

Another interesting feature in Fig. 10 is that, because of the nature of the chemical reaction, the waveform shape is such that multiple shocks form during propagation. It can also be seen that the distance between these shocks is decreasing as the wave propagates. Although it would require measurements at greater distances, it is probable that some of these shocks will eventually merge. Consequently, this demonstration could be used to motivate a class discussion of shock coalescence, which occurs in, e.g., sonic boom and nonlinear broadband noise propagation.³⁷

An additional observation can be made about the form of the nonlinear propagation shown in Fig. 10. The fact that removing spherical spreading effectively normalizes the waveforms is also evidence that the peak pressure decay is not nonlinear in the preshock region, which is predicted by the Earnshaw solution. This is further confirmed in Fig. 11, where the measured peak pressure closely aligns with linear, spherical geometric spreading theory based on the measured peak pressure at the closest microphone and an assumed source location at the center of the balloon.

VI. CONCLUSION

This article has shown that the explosion from a balloon filled with acetylene and oxygen produces a clear demonstration of important nonlinear phenomena, such as attenuation at shocks and waveform lengthening. Use of the Earnshaw solution to the lossless Burgers equation and weak-shock theory allows for a reasonable quantitative prediction of the evolution of waveform characteristics. It has also been shown for comparison that the explosion from a balloon filled with hydrogen and oxygen is another example where nonlinear theory is needed to explain the waveform steepening that occurs during wave propagation. Appropriate use of this demonstration should allow the advanced student in

physical acoustics to engage in the active learning of the mathematics of nonlinear phenomena.

ACKNOWLEDGMENTS

M.B.M. was supported by a Brigham Young University Mentoring Environment grant. Gordon L. Nielson and Julia A. Vernon are thanked for their help with the experiments. The peer reviewers are also thanked for their very insightful and helpful comments.

- ¹C. H. Crouch, A. P. Fagen, J. P. Callan, and E. Mazur, "Classroom demonstrations: Learning tools or entertainment?," *Am. J. Phys.* **72**, 835–838 (2004).
- ²D. R. Sokoloff and R. K. Thornton, *Interactive Lecture Demonstrations: Active Learning in Introductory Physics* (Wiley, Hoboken, NJ, 2004), pp. 1–374.
- ³D. A. Russell, "Basketballs as spherical acoustic cavities," *Am. J. Phys.* **78**, 549–554 (2010).
- ⁴M. D. Gardner, K. L. Gee, and G. Dix, "An investigation of Rubens flame tube resonances," *J. Acoust. Soc. Am.* **125**, 1285–1292 (2009).
- ⁵R. M. Keolian, "A demonstration apparatus of the cochlea," *J. Acoust. Soc. Am.* **101**, 1199–1201 (1997).
- ⁶G. C. Maling, Jr., "Simplified analysis of the Rijke phenomenon," *J. Acoust. Soc. Am.* **35**, 1058–1060 (1963).
- ⁷D. C. Thomas, K. L. Gee, and R. S. Turley, "A balloon lens: Acoustic scattering from a penetrable sphere," *Am. J. Phys.* **77**, 197–203 (2009).
- ⁸R. R. Boullosa and F. Orduña-Bustamante, "Acoustic levitation at very low frequencies," *Acta Acust.* **96**, 376–382 (2010).
- ⁹W. D. Hayes and H. L. Runyan, Jr., "Sonic-boom propagation through a stratified atmosphere," *J. Acoust. Soc. Am.* **51**, 695–701 (1970).
- ¹⁰K. L. Gee, V. W. Sparrow, M. M. James, J. M. Downing, C. M. Hobbs, T. B. Gabrielson, and A. A. Atchley, "The role of nonlinear effects in the propagation of noise from high-power jet aircraft," *J. Acoust. Soc. Am.* **123**, 4082–4093 (2008).
- ¹¹W. E. Baker, *Explosions in Air* (University of Texas Press, Austin, TX, 1973).
- ¹²M. Shaw and K. L. Gee, "Acoustical analysis of an indoor test facility for a 30-mm Gatling gun," *Noise Cont. Eng. J.* **58**, 611–620 (2010).
- ¹³L. Howle, D. G. Schaeffer, M. Shearer, and P. Zhong, "Lithotripsy: The treatment of kidney stones with shock waves," *SIAM Rev.* **40**, 356–371 (1998).
- ¹⁴R. O. Cleveland and O. A. Sapozhnikov, "Modeling elastic wave propagation in kidney stones with application to shock wave lithotripsy," *J. Acoust. Soc. Am.* **118**, 2667–2676 (2005).
- ¹⁵A. D. Pierce, *Acoustics: An Introduction to its Physical Principles and Applications* (Acoustical Society of America, Woodbury, NY, 1989), pp. 566–617.
- ¹⁶D. T. Blackstock, M. F. Hamilton, and A. D. Pierce, "Progressive waves in lossless and lossy fluids," in *Nonlinear Acoustics*, edited by M. F. Hamilton and D. T. Blackstock (Academic, San Diego, 1998), Chap. 4.
- ¹⁷D. T. Blackstock, "On plane, spherical, and cylindrical sound waves of finite amplitude in lossless fluids," *J. Acoust. Soc. Am.* **36**, 217–219 (1964).
- ¹⁸F. M. Pestorius and D. T. Blackstock, "Propagation of finite-amplitude noise," in *Finite-Amplitude Wave Effects in Fluids*, edited by L. Bjorno (IPC Science and Technology, Guildford, Surrey, UK, 1973), pp. 24–29.
- ¹⁹H. E. Bass, R. Raspet, J. P. Chambers, and M. Kelly, "Modification of sonic boom wave forms during propagation from the source to the ground," *J. Acoust. Soc. Am.* **111**, 481–486 (2002).
- ²⁰D. T. Blackstock, "Connection between the Fay and Fubini solutions for plane sound waves of finite amplitude," *J. Acoust. Soc. Am.* **39**, 1019–1026 (1966).
- ²¹H. W. Liepmann and A. Roshko, *Elements of Gas Dynamics* (Dover, New York, 2002), pp. 57–61.
- ²²S. Temkin, "Attenuation of guided, weak sawtooth waves," *J. Acoust. Soc. Am.* **46**, 267–271 (1968).
- ²³D. T. Blackstock, "Propagation of plane sound waves of finite amplitude in nondissipative fluids," *J. Acoust. Soc. Am.* **34**, 9–30 (1962).
- ²⁴For more on this topic, see Ref. 22 and F. M. Pestorius and S. B. Williams, "Upper limit on the use of weak-shock theory," *J. Acoust. Soc. Am.* **55**, 1334–1335 (1974).
- ²⁵P. H. Rogers, "Weak-shock solution for underwater explosive shock waves," *J. Acoust. Soc. Am.* **62**, 1412–1419 (1977).
- ²⁶D. T. Blackstock, "Propagation of a weak shock followed by a tail of arbitrary waveform," *Proceedings of the 11th International Congress on Acoustics, Paris, France* (1983), Vol. 1, pp. 305–308.
- ²⁷R. M. Corless, G. H. Gonnet, D. E. G. Hare, D. J. Jeffrey, and D. E. Knuth, "On the Lambert W function," *Adv. Comp. Math.* **5**, 329–359 (1996).
- ²⁸A conversation with D. T. Blackstock revealed that he actually used this problem as a homework assignment in his nonlinear acoustics course.
- ²⁹*MATLAB*, Release 2010 (The Mathworks, Inc., Natick, MA, 2010).
- ³⁰H. E. Bass, L. C. Sutherland, and A. J. Zuckerwar, "Atmospheric absorption of sound: Update," *J. Acoust. Soc. Am.* **88**, 2019–2021 (1990); H. E. Bass, L. C. Sutherland, and A. J. Zuckerwar, "Erratum: Atmospheric absorption of sound: Further developments," *J. Acoust. Soc. Am.* **99**, 1259 (1996).
- ³¹D. T. Blackstock, "Generalized Burgers equation for plane waves," *J. Acoust. Soc. Am.* **77**, 2050–2053 (1985).
- ³²M. F. Hamilton, Y. A. Il'inskii, and E. A. Zabolotskaya, "Dispersion," in *Nonlinear Acoustics*, edited by M. F. Hamilton and D. T. Blackstock (Academic, San Diego, 1998), Chap. 5.
- ³³K. L. Gee, J. A. Vernon, and J. H. Macedone, "Auditory risk of exploding hydrogen-oxygen balloons," *J. Chem. Ed.* **87**, 1039–1044 (2010).
- ³⁴W. J. Murphy and R. L. Tubbs, "Assessment of noise exposure for indoor and outdoor firing ranges," *J. Occup. Environ. Hyg.* **4**, 688–697 (2007).
- ³⁵T. B. Gabrielson, T. M. Marston, and A. A. Atchley, "Nonlinear propagation modeling: Guidelines for supporting measurements," *Proc. Noise-Con* **114**, 275–285 (2005).
- ³⁶ANSI S1.13-2005, *Measurement of Sound Pressure Levels in Air* (Acoustical Society of America, Melville, NY, 2005).
- ³⁷M. R. Shepherd, K. L. Gee, and M. S. Wochner, "Short-range shock formation and coalescence in numerical simulation of broadband noise propagation," *J. Acoust. Soc. Am.* **126**, 2886–2893 (2009).